Geosci. Instrum. Method. Data Syst. Discuss., 4, 385–434, 2014
www.geosci-instrum-method-data-syst-discuss.net/4/385/2014/
doi:10.5194/gid-4-385-2014

Geoscientific Instrumentation Methods and Data Systems Discussions
Open Access

Calibration of QM-MOURA three-axis magnetometer and gradiometer

M. Díaz-Michelena[1], R. Sanz[1,*], and M. F. Cerdán[1,2]

[1]Payolads and Space Sciences Department, National Institute of Aerospace Technology (INTA), Ctra. De Ajalvir km 4, 28850 Torrejón de Ardoz, Spain
[2]Earth Physics, Astronomy and Astrophysics I Department, Complutense University of Madrid, Pza. de las Ciencias, s/n, 28040 Madrid, Spain
[*]now at: CNR-IMM MATIS at Physics and Astronomy Department, Catania University, Via S. Sofia, 64, 95123 Catania, Italy

Received: 17 January 2014 – Accepted: 28 March 2014 – Published: 4 August 2014

Correspondence to: M. Díaz-Michelena (diazma@inta.es)

Published by Copernicus Publications on behalf of the European Geosciences Union.

Abstract

The MOURA instrument is a three axes magnetometer and gradiometer equipped with an inclinometer designed and developed for Mars MetNet Precursor mission.

The qualification model (MOURA QM) is devoted to magnetic surveys on Earth with the aim to achieve some experience prior to the arrival to Mars.

In this work it is presented a practical first approach for the calibration of the instrument for these preliminary field campaigns on Earth. Other works will describe the design, up-screening and qualification and full capabilities of the instrument in depth, giving some feedback on the development.

1 Introduction

MOURA is a three axis magnetometer and gradiometer instrument, to be included in the Spanish payload for the Finnish-Russian-Spanish Mars MetNet Precursor Mission (MMPM) (Mars MetNet Mission, 2014), rescheduled for 2018. The mission concept of MMPM is to deploy over the surface of Mars the first lander of a net of meteorological stations based on the penetrators concept. One of the targeted measurements of MOURA instrument will be to measure the change in remanence magnetization of Mars lithospheric minerals. We will search for temperature transitions for the compositional analysis of the crust (Sanz et al., 2011; Fernández et al., 2013) aiming to give explanation for its local magnetic anomalies, with intensities several orders of magnitude higher than the Earth ones.

Due to the limited development time (2 years), mass and energy constrains of the mission (150 g and < 0.5 W for the three Spanish payloads), MOURA followed a double design: one compact sensor with macroscopic front end electronics and a second with a mixed applied specific integrated circuit (ASIC) based front end (Sordo-Ibáñez et al., 2013). This work is focused on the former one. MOURA is located on top of the inflatable structure of the lander (Fig. 1) to provide a certain distance from the

GID
4, 385–434, 2014

penetrator, avoiding any extra mass for a deployment system. Therefore, apart from the two magnetometers (for close gradiometry) and the compensating temperature sensors, it has a tilt angle detector to determine the relative position respect to the horizontal.

The expected environmental conditions for MOURA include a storage temperature from −120 to 125 °C, operating temperatures between −90 and 20 °C and total irradiation doses up to 15 krad Si^{-1}. Because of the above mentioned mission constraints, both the sensing and the electronics suppose a trade-off between performance under that expected environment, power and mass budget. In addition, the magnetic signal of the electronic components was also carefully measured, in order to improve the magnetic cleanliness of the compact instrument (of a total mass of 72 g). As a result, the part list for the electronics was restricted according to their magnetic signal. Under the mentioned demanding criteria the selected sensing element was the tri-axial HMC1043 magnetic sensor by Honeywell (Honeywell Magnetic Sensors, 2014). The HMC1043 sensors belong to a family of sensors based on Anisotropic Magnetoresistance (AMR) effect (Freitas et al., 2007) which has been exhaustively up-screened (temperature, thermal shock, life cycle, and radiation) by INTA and successfully used in previous space missions (Sanz et al., 2012; Michelena et al., 2010; Michelena, 2009, DTUsat, 2014). Although the selection of HMC1043 for the two magnetic sensing elements presents advantages in terms of weight and power consumption, the AMR technology based sensors present several drawbacks like their resolution (lower compared with other sensing technologies, like the fluxgates), or an important dependence of their response (gain and offset) with temperature. This point is particularly important because MOURA is expected to be allocated outside the lander (Fig. 1) and thus, exposed to Mars surface thermal fluctuations. As one of the main objectives of MOURA is to measure the thermal variation of Martian magnetic minerals magnetization, this thermal characterization of the instrument becomes critical.

GID
4, 385–434, 2014

Other works, which report on the description and qualification, and on the electronic design of the instrument, will explain these improvements for the magnetometer in future papers.

Due to the necessities of the project, after the successful qualification (mechanical shock, vibration, thermal and vacuum), the qualification model (QM) of the magnetometer was slightly modified, and therefore should be strictly denominated engineering qualification model (EQM). This EQM is still fully representative (electric and functional) of the flight model (FM) but not mechanically representative. This fact will have implications in the calibration with temperature of the instrument.

In the present work we focus on the first calibrations performed to the MOURA EQM (MOURA from now on) as is (Fig. 2), which involves: magnetic, tilt angle detector, including gravity measurements characterization, and thermal behaviour. The purpose of this calibration is to have a representative and useful instrument for real field measurements on Earth (prospection, etc.) prior to the deployment of the MOURA FM on Mars. For this reason, the field range has been increased to ±65 µT (extendable to ±130 µT, see Table 1). The original range for Mars would be ±6.5 µT to cover the huge anomalies over the surface.

Finally we show a comparison of the corrected data registered by MOURA in the South of Spain, versus the nearest official magnetic daily variation data provided by San Pablo de los Montes Geomagnetic Observatory (IAGA code: SPT) (Geomagnetic observatories, 2014).

In forthcoming works we will also write on our real and long-term field measurement with MOURA in comparison with a scalar absolute magnetometer (Geometrics 858), and the interpretation, to describe the potential of this miniaturized compact magnetometers for rovers and balloons.

GID
4, 385–434, 2014

2 Devices and equipment

In this section a brief description of the tested instrument and employed devices are presented.

2.1 Brief description of MOURA and tested parameters

For the understanding of the present manuscript Table 1 summarizes the main magnetic characteristics of MOURA. This table is discussed in depth in the above mentioned parallel work where we will discuss the operation of the sensor for the optimization of the flip and measurement timing with temperature.

MOURA uses the SET/RESET flip recommended by the manufacturer (Honeywell Magnetic Sensors, 2014) and therefore, the measurement will consist in the subtraction of the two mirror states (after the SET and RESET pulses).

In addition MOURA includes two temperature sensors for the sensors compensation in contact with the magnetic sensors (glued to the package of the HMC1043), and a three axis accelerometer ADXL327 by Analog Devices, for the determination of the relative orientation of MOURA. The accelerometer is selected amongst other devices because of its lower magnetic signature (magnetic moment lower than 1 $\mu A\,m^2$ when exposed to moderate fields (100 μT) contributing less than 0.5 nT in the position of the sensor).

For the present characterization we focus on the signals described in Table 2 (denoted as channels).

As it has been introduced, the magnetic signals are obtained after the application of SET/RESET pulses ($V_{S/R}$ and $I_{S/R}$) on the magnetoresistive sensing elements in order to avoid cross axis effects, increase repeatability by decreasing the thermal disorder of magnetic domains, and reduce hysteresis (Honeywell Magnetic Sensors, 2014).

GID
4, 385–434, 2014

2.2 Employed equipment

All the calibration has been performed in the Space Magnetism Laboratory at INTA headquarters with the exception of the magnetic daily variations, which were registered in Almuñécar, locality in the South of Spain.

Controlled magnetic fields are generated by a set of three pairs of high mechanical precision Helmholtz coils (HC), model Ferronato BH300-A. Each pair of coils (denoted as HC_X, HC_Y and HC_Z) is calibrated by means of Bartington FG100 fluxgate (certified by Bartington, against the calibration references, in accordance with ISO10012: Mag-01 magnetometer, Mag Probe B, solenoid with current source and DC scaling solenoid, see Table 3). The coils constants are: $HC_X = 524.38\,\mu T\,A^{-1}$, $HC_Y = 542.15\,\mu T\,A^{-1}$, and $HC_Z = 525.6\,\mu T\,A^{-1}$. The electric currents to generate the magnetic fields are supplied by a Keithley 6220 precision current source.

Non-orthogonalities in the HC are lower than 4″; according to the documentation provided by the manufacturer (Honeywell Magnetic Sensors, 2014), orthogonality between X-Y axes is better than 3.6″ and it is checked experimentally that between the Z axis and the XY plane the non-orthogonality is below 0.5°.

For monitoring magnetic field pulses a fluxgate magnetometer FG-500 is used (see Table 3).

A thermal chamber (Binder MK53) is employed to set and control the temperature during the characterization tests. This chamber allows to apply temperatures from −70 to 180 °C, and to circulate dry N_2 gas inside of the chamber in order to control the humidity of the atmosphere. The N_2 flow is kept between 1 and 5 L min^{-1}. The measurement of the atmospheric humidity inside the chamber is performed by a Vaisala HMI31 humidity and temperature indicator, and always kept under 18 %. This is done to prevent water condensation in the low temperature range. It is not observed any influence of humidity on our sensors' performance.

For the characterization tests, the temperature register is performed by the included thermal chamber temperature sensors, those included in MOURA and two

GID
4, 385–434, 2014

additional temperature sensors. These additional temperature sensors are two PT-1000 resistances calibrated by means of a SIKA TP 38165E, and connected to a data acquisition system (Agilent 3497A Automatic DAS, computer commanded).

For the calibration of the inclinometer it is used a sine bar and gauge blocks with values between 1.5 and 141 mm to generate the desired tilt angles around X and Y axes (α and β angles). The rotations are obtained with one of the cylindrical plugs leaning on the gauge blocks and the other on the surface plate. The accuracy of the method is better than 10 min of arc.

3 Methods and results

In this section it is described the procedure followed for MOURA calibration.

The results shown here correspond to the measurements taken with the flipping operation. Therefore, the response of the i axis (of the six measuring axes of the magnetometer): $B_{\mathrm{MOURA},i}$ corresponds to:

$$\frac{(\mathrm{SET}_i - \mathrm{RESET}_i)}{2 \cdot \mathrm{VREG}} = \cos\theta_i \cdot B_{\mathrm{REAL}} \cdot \mathrm{GAIN}_i - \mathrm{OFFSET}_i \quad (1)$$

where $i = \mathrm{X1}, \mathrm{X2}, \mathrm{Y1}, \mathrm{Y2}, \mathrm{Z1}, \mathrm{Z2}$. SET_i and RESET_i are the registered magnetic signals from a given axis "i" after the application of a SET and RESET pulse, respectively. VREG is the registered voltage sourcing the magneto-resistive bridge. α_i is the angle between the direction of the field and the measurement direction of "i" sensor. $\mathrm{B_{REAL}}$ is the external magnetic field. GAIN_i is the effective gain of the "i" sensor. OFFSET_i is the offset of the "i" sensor.

The sensor always acquire both Set and Reset data and thus, it is always possible to use this same calibration data for the data without flipping.

Firstly, the sensors are calibrated at room temperature. The calibration consists in the offset, gain, non-orthogonalities and Euler angles characterization.

Secondly, the sensors were calibrated in temperature.

GID
4, 385–434, 2014

MOURA temperature sensors had been previously calibrated by means of a 38165E system by SIKA TP giving rise to a polynomial fit. However, this calibration is not used in the present work, but the calibration is performed with the direct readings of the temperature sensors no matter the real temperature.

Also it has to be noticed that to avoid influence of the voltage source fluctuations, the output values are always normalized with the bridge voltage, which is monitored.

The parameters affected by temperature are:

1. Gain
2. Offset.

Therefore, MOURA response (for one of its axis) to a real magnetic field can be expressed as:

$$B_{\mathrm{MOURA}}(T)_i = \cos\theta_i \cdot B_{\mathrm{REAL}} \cdot \mathrm{GAIN}_i \cdot (1 - \Delta GAIN_i \cdot (T - T_{\mathrm{G}})) - \mathrm{OFFSET}_i \cdot (1 - \Delta\mathrm{OFFSET}_i \cdot (T - T_{\mathrm{OFFSET}})) \quad (2)$$

where $\Delta\mathrm{GAIN}_i$ is the normalized GAIN temperature variation rate. $\Delta\mathrm{OFFSET}_i$ is the normalized OFFSET temperature variation rate. T_{G} is the reference temperature for the gain, i.e. normalization temperature for GAIN_i. T_{OFFSET} is the reference temperature for the offset, i.e. normalization temperature for OFFSET_i.

From now on we will use M_i to refer to the "i" sensor measurement and leave $\mathrm{B}_{\mathrm{MOURA}}$ for the total magnetic vector.

3.1 Room temperature characterization

In this section it is described the room temperature characterization of the offsets, gains and output field generated by the inner coils.

GID
4, 385–434, 2014

3.1.1 Characterization of MOURA magnetic offsets at room temperature

The offset characterization of the two magnetic sensors components was performed inside a 3-layered magnetic shielded chamber of 2.5 m^3, previously characterized (at different points) by means of a three axes fluxgate with minimum detectable fields in the order of 10 pT.

Because the magnetic field inside the chamber (~ 0.1 nT) is lower than the minimum detectable field of the sensor (~ 1 nT), passive compensation of the Earth magnetic field was considered to be sufficient.

After warming up and thermal stabilization at room temperature (TMP1 = $18.13 \pm 0.03\,^{\circ}$C and TMP2 = $19.21 \pm 0.03\,^{\circ}$C, with variations $< 0.1\,^{\circ}\mathrm{C\,min^{-1}}$), MOURA data were acquired constantly during the whole process.

Magnetic sensors outputs were analyzed. Mean values and standard deviations are shown in Table 4.

3.1.2 Non-orthogonalities and Euler angles determination – gain characterization

In this section we describe the procedure and results for the determination of the geometrical directions of MOURA sensors axes.

The registered signal of MOURA "i" sensor, M_i, at room temperature can be written in vector expression as:

$$\begin{aligned} M_i &= (\boldsymbol{B}_{\mathrm{REAL}} \cdot \boldsymbol{u}_i) \cdot \mathrm{GAIN}_i - \mathrm{OFFSET}_i; \\ \boldsymbol{B}_{\mathrm{real}} \cdot \boldsymbol{u}_i &= |\boldsymbol{B}| \cdot |\boldsymbol{u}_i| \cdot \cos\theta_i; \\ M_i &= |\boldsymbol{B}| \cdot \cos\theta_i \cdot \mathrm{GAIN}_i - \mathrm{OFFSET}_i. \end{aligned} \tag{3}$$

Being $\boldsymbol{u}_i$ a unit vector in the measuring direction of "i" sensor.

The external field, B_{REAL}, is generated in the zero field chamber by the previously described set of HC. The sensor box is aligned with the axes of the HC. Hereinafter,

GID
4, 385–434, 2014

MOURA basis will refer to the measuring directions of each three axis sensor, and not to the box. Notice that the magnetic field generated by the HC in the HC basis will be denoted by B and the measurements of MOURA in MOURA basis will be denoted by M (Fig. 3).

If θ_A and $GAIN_A$ are unknown it is not possible to distinguish between a misalignment and a scale factor.

To simplify the problem and to calculate the most accurate values of the GAIN and misalignment of sensors with the external system of reference (HC) some approximations can be applied:

1. The three axes of the magnetometers and the HC are taken as orthogonal due to its construction properties, described in Sect. 2.2.
2. The change of basis between HC and MOURA reference systems can be taken as a composition of small rotations around axes of the external reference system. Under this approximation it is not required the use of an unknown rotation matrix.
3. Gains of the different axes of the same sensor have similar values.

For each three axes magnetometer (1 and 2), the angle between B_X and M_X is denoted as α_x, between B_Y and M_Y as β_y and B_Z andM_Z as γ_z. Notice that these angles have both contributions: the already known non-orthogonality of the coils and the Euler angles referred to the HC system. These angles have to be determined for the two magnetometers composing the gradiometer.

In contrast with other highly precise calibration methods (Renaudin et al., 2010; Petrucha and Kaspar, 2009; Petrucha et al., 2009; Cai et al., 2010), in which a well calibrated and aligned three-axis goniometric platform is used, in the present case we have employed a method based on the calibration by means of the application of time varying circular magnetic fields (harmonic with a $\pi/2$ phase shift between components) around MOURA, in the planes of the HC system. As a result of these sine-cosine circular fields, an elliptical response, due to the expected misalignment and different gain of each sensor axis, will be detected by MOURA sensors.

GID
4, 385–434, 2014

MOURA was fixed in the centre and aligned with the set of HC, taking as a reference the geometrical shape of its box: for this measurement, a high-precision container was made ad hoc in order to fit and immobilize the magnetometer, and a set of laser theodolites was used to align HC and the sides of the container. Doing so, we could set MOURA and the set of HC in co-axial position, with a calculated misalignment below $0.1'$.

The whole set was placed into the magnetic shielded chamber.

The performed calibration sequence, based in the approximations mentioned above, was as follows:

- MOURA switch-on
- Warming up
- Temperature equilibrium (thermal variations $\leq 0.2\,^{\circ}\mathrm{C\,min^{-1}}$)
- Application of a rotating magnetic field in the HC XY plane (see Table 5)
- Synchronized MOURA data monitoring
- Application of a rotating magnetic field in the HC ZX plane (see Table 5)
- Synchronized MOURA data monitoring
- Application of a rotating magnetic field in the HC YZ plane (see Table 5)
- Synchronized MOURA data monitoring
- MOURA registered data are compared to those of the applied magnetic field (Fig. 4)

GID
4, 385–434, 2014

– Misalignment measurement by means of a linear fit of the signal arctangents between both systems in the three planes:

$$\Omega_{\mathrm{HC}_{ij}}\,(\mathrm{step}) = \arctan\left(\frac{B_i}{B_j}\right);$$

$$\Omega_{\mathrm{MOURA}_{i'j'}}\,(\mathrm{step}) = \arctan\left(\frac{B_{i'}}{B_{j'}}\right);$$

$$\Omega_{\mathrm{HC}_{ij}} = \delta + P \cdot \Omega_{\mathrm{MOURA}_{i'j'}} \tag{4}$$

where B_i is the magnetic field produced by pairs of HC "i". B_j is the magnetic field produced by pairs of HC "j". $B_{i'}$ is the magnetic field registered by axis "i" of MOURA. $B_{j'}$ is the magnetic field registered by axis "j" of MOURA. δ is de misalignment between ij and $i'j'$ axis (HC axes and MOURA axes). P is the slope of the linear fitting between $\Omega_{\mathrm{HC}_{ij}}$ and $\Omega_{\mathrm{MOURA}_{i'j'}}$.

– Application of a positive pulse of 60 mA in the X direction (P_x^+), 1 min duration

– Application of a negative pulse of 60 mA in the X direction (P_x^-), 1 min duration

– Application of a positive pulse of 60 mA in the Y direction (P_y^+), 1 min duration

– Application of a negative pulse of 60 mA in the Y direction (P_y^-), 1 min duration

– Application of a positive pulse of 60 mA in the Z direction (P_z^+), 1 min duration

– Application of a negative pulse of 60 mA in the Z direction (P_z^-), 1 min duration

– Room temperature GAIN_x, GAIN_y, GAIN_z calculation by comparison of the MOURA registered magnetic signals and reference signals moduli using:

$$B_{\mathrm{MOURA}}(T)_i^+ - B_{\mathrm{MOURA}}(T)_i^- = \cos\theta_i \cdot \left(P_i^+ - P_i^-\right) \cdot \mathrm{GAIN}_i \cdot (T_{\mathrm{G}}). \tag{5}$$

GID
4, 385–434, 2014

Note that X1 and Y1 have opposite sense directions than X2 and Y2, respectively for engineering purposes.

The results from the fittings are presented in Table 6.

Once the linear fitting and then the misalignment angles between planes were obtained, it was possible to approximate the misalignment of each axis by direct composition. Under this approximation the gains for each axis were obtained by direct calculus employing Eq. (5) and statistical corrections of the measured magnetic moduli. The results are shown in Table 7.

With this correction, relative errors in the measurement of the field with the different axes are below 0.3 % except for the case of the Y1 sensor, which has an error of up to 0.9 %.

3.1.3 Characterization of output fields of the inner coils

The characterization of the inner coils constant (field vs. current) needs to be performed since the field vs. current provided by the manufacturer is subject to an error and these coils are used for the calibration of the sensors prior to the use. Also these coils are used to extend the dynamic range of the magnetometer when it is saturated in the automated mode.

This characterization is performed in the same conditions as the gain characterization (using the same HC system in the zero field chamber).

Decreasing and increasing field ramps are applied in 126 steps (between −45 655 and 45 665 nT). At room temperature the field generated by the different inner coils is between 0.8293 and 0.8767 ± 0.0003 times to that generated by the external field. More details will be given in Sect. 3.2.3, where the temperature calibration data are shown.

GID
4, 385–434, 2014

3.1.4 Inclinometer and gravimeter characterization

In order to be able to derive the horizontal and vertical components of the field and thus its orientation, it was required to characterize the tilt angle detector response, three-axis accelerometer. This calibration is not direct since the accelerometer is placed on a PCB tilted 45° over the horizontal and rotated an angle −90° respect to MOURA box Z axis, and 45° respect to MOURA Y axis. This rotation aims to linearize the accelerometer components response at zero tilt.

Also for field work it is interesting to characterize the gravity measurements in order to complement the magnetic measurements with gravity (low resolution) ones.

The following procedure designed by INTA and named: Procedure of Measurement Levels Calibration, consisted in the comparison between the real inclinations of the sine bar around X and Y axes (α and β angles) with the measurements provided by the accelerometer axis (Table 8). The sequence of tilt is: zero tilt – maximum tilt – minimum tilt (negative) – zero tilt with five different values of tilt in absolute value.

The accelerometer and MOURA box system systems of reference are designed by: {ACC} and {MOU}, respectively.

The theoretical change of basis matrix "**B**" between {ACC} and {MOU} and the inverse "$\mathbf{B}^{-1}$", with their respective errors, are:

$$\mathbf{B} = \frac{1}{2}\begin{bmatrix} \sqrt{2} & 1 & 1 \\ -\sqrt{2} & 1 & 1 \\ 0 & -\sqrt{2} & \sqrt{2} \end{bmatrix}; \quad \Delta\mathbf{B} = \begin{bmatrix} 0.0371 & 0.0524 & 0.0524 \\ 0.0371 & 0.0524 & 0.0524 \\ 0 & 0.0371 & 0.0371 \end{bmatrix} \tag{6}$$

$$\mathbf{B}^{-1} = \frac{1}{2}\begin{bmatrix} \sqrt{2} & -\sqrt{2} & 0 \\ 1 & 1 & -\sqrt{2} \\ 1 & 1 & \sqrt{2} \end{bmatrix}; \quad \Delta\mathbf{B}^{-1} = \begin{bmatrix} 0.0371 & 0.0371 & 0 \\ 0.0524 & 0.0524 & 0.0371 \\ 0.0524 & 0.0524 & 0.0371 \end{bmatrix}. \tag{7}$$

Table 9 displays the relative errors between the measured and theoretical values of α. The measured error permits to calculate a slight extra rotation around Z axis (an angle of −1.7686°) due to the experimental positioning of the accelerometer PCB.

GID
4, 385–434, 2014

The new change of basis matrix corresponds to:

$$\mathbf{B}_{\text{exp}} = \mathbf{B}\mathbf{R}_{\varepsilon} = \frac{1}{2}\begin{bmatrix} \sqrt{2} & 1 & 1 \\ -\sqrt{2} & 1 & 1 \\ 0 & -\sqrt{2} & \sqrt{2} \end{bmatrix}\begin{bmatrix} 0.9995 & -0.0309 & 0 \\ 0.0309 & 0.9995 & 0 \\ 0 & 0 & 1 \end{bmatrix}. \quad (8)$$

Notice that this matrix will have to be characterized for each experimental set up, i.e. each model will have its own change of basis matrix.

Experimental values of α and β obtained subtracting the zero tilt measurement from those corresponding to the different inclinations can be adjusted easily to the real tilt values giving:

$$\alpha_{\text{EXP}}(^\circ) = 1.0894 \cdot \alpha_{\text{ref}}(^\circ) + 0.7268^\circ \quad (9)$$

$$\beta_{\text{EXP}}(^\circ) = 0.9779 \cdot \beta_{\text{ref}}(^\circ) - 1.7475^\circ. \quad (10)$$

But these values have a slight difference with those derived from the accelerometer measurements in MOURA box reference system:

$$\alpha'_{\text{EXP}}(^\circ) = \arctan\left(\frac{\text{MOU\_Y}}{\text{MOU\_Z}}\right) = \alpha_{\text{EXP}}(^\circ) - 7.2890^\circ \quad (11)$$

$$\beta'_{\text{EXP}}(^\circ) = -\arctan\left(\frac{\text{MOU\_X}}{\text{MOU\_Z}}\right) = \beta_{\text{EXP}}(^\circ) + 21.4369^\circ. \quad (12)$$

Consequently, the equations for the real inclinations around X and Y axes from the accelerometer measurements in MOURA box reference system are:

$$\alpha(^\circ) = 0.9179 \cdot \arctan\left(\frac{\text{MOU\_Y}}{\text{MOU\_Z}}\right) + 6.0237^\circ \quad (13)$$

$$\beta(^\circ) = -1.0226 \cdot \arctan\left(\frac{\text{MOU\_X}}{\text{MOU\_Z}}\right) - 20.1347^\circ. \quad (14)$$

GID
4, 385–434, 2014

These data permit the determination of the inclination with errors up to 3 % in α for $-30^\circ < \alpha < 30^\circ$, and of 6 % in $-30^\circ < \beta < 30^\circ$. A better adjust with errors up to 1 % in α for $-40^\circ < \alpha < 40^\circ$, and of 3 % in $-40^\circ < \beta < 40^\circ$, can be obtained with the following polynomial fit (Fig. 5):

$$\alpha(^\circ) = -0.0012 \cdot \arctan^2\left(\frac{\text{MOU\_Y}}{\text{MOU\_Z}}\right) + 0.8921 \cdot \arctan\left(\frac{\text{MOU\_Y}}{\text{MOU\_Z}}\right) + 6.5543^\circ \quad (15)$$

$$\beta(^\circ) = 0.0038 \cdot \arctan^2\left(\frac{\text{MOU\_X}}{\text{MOU\_Z}}\right) - 0.8656 \cdot \arctan\left(\frac{\text{MOU\_X}}{\text{MOU\_Z}}\right) - 20.3296^\circ. \quad (16)$$

Also the gravimeter readings need to be calibrated since they are very dependent on the tilt angle measurements.

Without correction the errors in the gravity modulus are of 1 % for $\alpha = \pm 10^\circ$, but in the order of 5 % in $\beta = \pm 10^\circ$. By means of a quadratic correction with the tilt angles and considering that α and β are totally independent, the error is reduced to ± 0.0001 g (0.01 %) for $\alpha = \pm 40^\circ$ and ± 0.004 g (0.4 %) for $\beta = \pm 40^\circ$ ($g = 9.8\,\text{m}\,\text{s}^{-2}$).

3.2 Temperature dependent characterization

It is known that most of magnetic sensors have a temperature dependent response, and therefore, magnetic sensors need to undergo a temperature characterization when they are used in conditions of changing temperatures. Also the response of the conditioning electronics can change mostly when subject to huge temperature fluctuations.

The issue then is to determine the temperature of the devices (core of the sensor, amplifiers . . .) whose response varies with the temperature. This is a very complicated problem since normally the only accessible part of the devices is the package, the encapsulation. In the steady state of measurements (thermal dynamic equilibrium), the temperature of the package can be assumed as an indicator of the core temperature, though this can have a non negligible error when there are temperature gradients

GID
4, 385–434, 2014

or/and fast temperature variations with time. Also the flipping of the AMR sensors implies temperature variations of the core. This situation makes it necessary to find an optimal working mode, which is a trade-off between thermal changes, acquisition frequency and samples to average.

In this work we focus on a practical solution consisting in the characterization of the thermal behaviour in the steady state. Therefore, we focus on the two temperature channels, namely TMP1 and TMP2, corresponding to temperature sensors placed on top of the magnetic sensors. As it has been introduced, these temperature sensors were not in close contact with the active sensing element of the magnetic sensors i.e. magnetoresistive bridges, and therefore, they are not expected to provide an accurate measurement of the magnetic sensors instant temperatures. In addition, in this work it is considered that the orientation angles do not change by means of thermal expansions and contractions. This assumption responds to the fact that the calculated maximum angle deviation due to the worst case of an anisotropic thermal expansion is 0.015° approximately, in the order of the resolution limit of the sensor.

3.2.1 Offset characterization with temperature

The variation of the offset with temperature was formerly estimated with the daily fluctuation of the temperature outside the building (10–30 °C). It was observed that the variation of the offset with temperature was very similar to that of the gain. This test was performed inside a shielding chamber with a field stability that is better than 1.5 nT. Therefore the offset observed is only attributed to the variations of temperature inside the chamber, which are registered and are in good correlation with the offset values monitored. Consequently for the extended range of temperature, both variations with temperature will be considered equivalent, i.e. $\Delta OFFSET = \Delta GAIN$.

GID
4, 385–434, 2014

3.2.2 Gain characterization with temperature – V_{REG} compensation

The extended expression of Eq. (1), the expression of the measured fields in the different axes, as a function of temperature is:

$$M_{\mathrm{i}} = (\boldsymbol{B}_{\mathrm{REAL}} \cdot \boldsymbol{u}_i) \cdot \mathrm{GAIN}_i (1 - \Delta\mathrm{GAIN}(T - T_{\mathrm{G}}))$$
$$- \mathrm{OFFSET}_i (1 - \mathrm{OFFSET}_i (T - T_{\mathrm{OFFSET}}));$$
$$\boldsymbol{B}_{\mathrm{REAL}} \cdot \boldsymbol{u}_i = |\boldsymbol{B}| \cdot |\boldsymbol{u}_i| \cdot \cos\theta_{B_{\mathrm{REAL}} M_i};$$
$$M_i = |\boldsymbol{B}| \cdot \cos\theta_{B_{\mathrm{REAL}} M_i} \cdot \mathrm{GAIN}_i (1 - \Delta\mathrm{GAIN}(T - T_{\mathrm{G}}))$$
$$- \mathrm{OFFSET}_i (1 - \Delta\mathrm{OFFSET}_{\mathrm{A}} (T - T_{\mathrm{OFFSET}})). \quad (17)$$

Since the magnetic noise into the thermal chamber is higher than the precision of MOURA, it is not possible to control or monitor the magnetic field with the required precision and to discern absolute variations in the offset (OFFSET) and gain (GAIN) of MOURA. However it is possible to calculate the variation of the relative gain ($\Delta\mathrm{GAIN}_i$) by the measurement of the variation of the controlled amplitude between two applied magnetic pulses with same modulus and direction but opposite polarization, assuming that the variation of the external magnetic field is much slower than the duration of the pulses. These pulses are denoted as P^+ and P^- (see Fig. 6).

MOURA sensors response for P^+ and P^- pulses will be denoted by: $B_{\mathrm{MOURA}}(T)_i^+$ and $B_{\mathrm{MOURA}}(T)_i^-$, respectively:

$$B_{\mathrm{MOURA}}(T)_i^+ = \cos\theta_i \cdot P^+ \cdot \mathrm{GAIN}_i \cdot (1 - \Delta\mathrm{GAIN}_i \cdot (T - T_{\mathrm{G}}))$$
$$- \mathrm{OFFSET}_i \cdot (1 - \Delta\mathrm{OFFSET}_i \cdot (T - T_{\mathrm{OFFSET}}))$$
$$B_{\mathrm{MOURA}}(T)_i^- = \cos\theta_i \cdot P^- \cdot \mathrm{GAIN}_i \cdot (1 - \Delta\mathrm{GAIN}_i \cdot (T - T_{\mathrm{G}}))$$
$$- \mathrm{OFFSET}_i \cdot (1 - \Delta\mathrm{OFFSET}_i \cdot (T - T_{\mathrm{OFFSET}})). \quad (18)$$

Subtracting the pulses:

$$\frac{B_{\mathrm{MOURA}}(T)_i^+ - B_{\mathrm{MOURA}}(T)_i^-}{2} = \cos\theta_i \cdot |2P| \cdot \mathrm{GAIN}_i \cdot (1 - \Delta\mathrm{GAIN}_i \cdot (T - T_{\mathrm{G}})) = M_i^A(T) \quad (19)$$

GID
4, 385–434, 2014

where M_i^A is the averaged amplitude of the magnetic pulses measured by the i axis of MOURA.

The magnetic field pulses are monitored by means of a three axes fluxgate (FG-500). The accuracy of the magnetic field depends on the current in the circuit, which is controlled better than 1 ‰. Although it is not possible to determine analytically the absolute GAIN_i and θ_i, i.e. the metrics and orthogonal projection from the HC system to reference system of MOURA, it is possible to normalize the obtained signals using for the normalization the signal obtained at a chosen temperature (T_G):

$$M_i^A(T)/M_i^A(T_\mathrm{G}) = \frac{\cos\theta_i \cdot |P| \cdot \mathrm{GAIN}_i \cdot (1 - \Delta\mathrm{GAIN}_i \cdot (T - T_\mathrm{G}))}{\cos\theta_i \cdot |P| \mathrm{GAIN}_i \cdot (1 - \Delta\mathrm{GAIN}_i \cdot (T_\mathrm{G} - T_\mathrm{G}))};$$

$$M_i^A(T)/M_i^A(T_\mathrm{G}) = (1 - \Delta\mathrm{GAIN}_i \cdot (T - T_\mathrm{G})). \quad (20)$$

Applying a linear fitting of the normalized signals as a function of $T - T_\mathrm{G}$ it is possible to calculate $\Delta\mathrm{GAIN}_i$ as a function of temperature.

The test is carried out at six temperature values in the range of temperatures in which field measurements were performed, using as first reference the thermal chamber temperature controller: −60, −30, 0, 15, 45, and 60 °C. The registered humidity inside the chamber is < 18 % for the test (as explained in Sect. 2.2). The square magnetic pulses along the six semi-axis were applied by a nominal current of 10 mA supplied to the three pairs of HC simultaneously. The amplitude of each magnetic pulse was taken as the mean absolute value of each pulse applied along the same axis (positive and negative pulse). The registered magnetic field amplitudes were normalized to that obtained at room temperature: TMP1 = 25.9 ± 0.2 °C and TMP2 = 25.6 ± 0.2 °C. Two additional temperature sensors (calibrated PT-1000, denoted as TT and TL) were placed on the top (TT) and on a side (TL) of MOURA in order to guarantee thermal equilibrium. Since the level of magnetic noise generated by the hardware of the thermal chamber (mainly rotor and pumps) makes it impossible to obtain suitable accurate data, the thermal chamber was switched-off when the pulses were applied (Fig. 7).

GID
4, 385–434, 2014

The set-up and performed steps for the test comprised the following protocol:

- Placement of FG500, TT, TL and MOURA inside the geometric centre of the three pairs of HC. FG500, MOURA and HC axis were co-axial positioned
- Placement of the whole set inside the thermal chamber
- Warming up
- Start the acquisition of FG500, TT, TL, and MOURA
- Start the flow of N_2 to keep the humidity $< 18\,\%$
- Switch-on the thermal chamber
- Temperature selection (from here on, repeated for all temperature steps)
- Waiting time until thermal equilibrium is reached. Algorithm measuring an indicator of the temporal variation of registered temperature values by TT, TL, TMP1 and TMP2. The allowed temperature variation rate is $< 0.1\,^{\circ}\mathrm{C\,min^{-1}}$ (Table 10)
- Switch-off the thermal chamber
- Switch-on the pulses P^+ with the three pairs of HC by means of a Keithley precision source (square magnetic pulses, 1 min of duration, with a delay of 1 min between each positive and negative pulse)
- Measurement of all magnetic channels
- Switch-off the magnetic field generated with the HC from the Keithley precision source.
- Switch-on the pulses P^- with the three pairs of HC by means of a Keithley precision source (square magnetic pulses, 1 min of duration, with a delay of 1 min between each positive and negative pulse)

GID
4, 385–434, 2014

– Measurement of all magnetic channels

– Switch-off the magnetic field generated with the HC from the Keithley precision source.

These variations of temperature affect the voltage sourcing of the magnetoresistive bridges. VREG has a variation with temperature of 0.1 %. The variation is recorded and will also be taken into account for the response correction.

The obtained values of amplitude for each axis were normalized by those obtained at TMP1 = 25.9 °C and TMP2 = 25.6 °C. These normalized amplitudes were linearly fitted with the corresponding temperature (T – 25.9 °C for Sensor 1 data and T – 25.6 °C for Sensor 2 data) (see Fig. 8).

ΔGAIN values, derived from these fits, are presented in Table 11. For example: $\Delta GAIN_{X1} \cdot (T - T_G) = (-0.00370 \pm 5 \cdot 10^{-5})\,^{\circ}C^{-1} \cdot [TMP1(^{\circ}C) - 25.9\,^{\circ}C]$.

The coefficients for the thermal drift correction of the magnetic data for each axis are summarized in Table 12.

3.2.3 Inner coils characterization with temperature

In this section it is calibrated the thermal variation of the inner coils constant ($nT\,nT^{-1}$ or $nT\,mA^{-1}$). For simplicity only sensor 1 parameters are displayed.

This characterization is performed by means of a relative measurement of the constant variation with temperature and then referred to the temperature of reference in a similar way of the gain characterization with temperature.

In this case, two ramps have been applied with the inner coils:

– Ramp I: a linear decreasing magnetic field from 45 665 to −45 665 nT (applying 4.5665 mA) in 126 steps (measurements)

– Ramp II: a linear increasing magnetic field ramp from −45 665 to 45 665 nT in other 126 steps.

GID
4, 385–434, 2014

Previously it has been checked that the current passing through the inner coils do not increase the temperature of the magnetoresistors and thus, it does not alter the response.

In order to obtain the values of the inner coil constant variation with temperature ($(nT\,nT^{-1})/^{\circ}C$), the above mentioned magnetic field ramps were applied at the 5 different temperatures in the same thermal chamber as the previous test.

In this case, MOURA temperature sensors were also employed to register the temperature variation during the test.

The set-up and performed steps for the test comprised the following protocol:

- Placement of MOURA inside the thermal chamber.
- Start the flow of N_2 to keep the humidity < 18 %.
- Switch-off the thermal chamber
- Temperature selection (from here on, repeated for all temperature steps).
- Waiting time until thermal equilibrium is reached. Algorithm measuring an indicator of the temporal variation of registered temperature values by TT, TL, TMP1 and TMP2. The allowed temperature variation rate is $< 0.1\,^{\circ}C\,min^{-1}$.
- Switch-off thermal chamber.
- Application of magnetic field RAMP I and measurement of all channels
- Application of magnetic field RAMP II and measurement of all channels

An example of the obtained data is presented in Fig. 9. As it can be noted the offset value is higher than the obtained in the magnetic shielded chamber due to the lack of a magnetic clean environment.

The obtained coils constants for sensor 1 from the linear fits for each ramp at different temperatures, and averaging data corresponding to Ramp I and Ramp II, are presented in Table 13 and represented in as a function of TMP1.

GID
4, 385–434, 2014

The obtained Gains for each temperature were linearly fitted versus the registered temperature by TMP1 sensor (Fig. 10).

The thermal variations of the inner coils constants are presented in Table 14. For example: $\Delta\text{Constant}_{X1}(\text{nT nT}^{-1}) \cdot (\text{TMP1} - T_{\text{ref}})(^{\circ}\text{C}) = (-0.088034 \pm 7 \times 10^{-6})\,^{\circ}\text{C}^{-1} \cdot (\text{TMP1} - 25.9)(^{\circ}\text{C})$.

4 Measurement of the daily variation of the Earth magnetic field

In order to perform a preliminary test of the suitability of MOURA for field works, the instrument was deployed to measure the daily variation of the Earth magnetic field. The approximate coordinates of the deployment site were 36°44′2″ N, 3°41′28″ W, close to the sea level.

The magnetic data acquisition from MOURA was performed each 30 s SET/RESET, selecting all channels and 128 data averaging. UTC was used as a reference time. The obtained data were corrected and fitted with the previously obtained thermal correction parameters and compared with the geomagnetic data from San Pablo de los Montes Geomagnetic Observatory (DTUsat, 2014), approximate coordinates 39°33′00″ N, 4°21′00″ W and 922 m over the sea level. These data have been taken as a reference of the daily variation of the Earth magnetic field but they cannot be taken as an absolute reference of the Earth magnetic field due to the different position of the observatory and the possible environmental magnetic interferences, e.g. geomagnetic and human disturbances, in the surroundings of MOURA.

The daily Earth magnetic field variation measurements were performed during the days 26, 27, and 28 August 2012.

The daily variations of the Earth magnetic field were taken as the subtraction of the average modulus of the magnetic field (in all the considered time period) from the instant registered signal from MOURA and San Pablo de los Montes Geomagnetic Observatory. The average modulus of the magnetic field during that period of time was 44 279 nT. The results of the daily variation of the Earth magnetic field are shown in Fig. 11. Further experiments will compare the in situ measurements of

GID
4, 385–434, 2014

MOURA based at San Pablo de los Montes observatory with the observatory reference magnetometers.

5 Conclusions

A practical calibration of MOURA magnetometer and gradiometer has been performed with the aim of correcting previous field surveys on Earth. Offsets, gains, non-orthogonalities and Euler angles, and their variations with temperature have been characterized for the qualification model in a restricted temperature range from 0 to 60 °C. Also the tilt angle detector has been characterized and the gravity measurements compensated.

Finally it has been performed a comparison of MOURA measurements along a couple of days with the Earth magnetic field daily variations recorded by the magnetometers of a geomagnetic observatory.

Results are in agreement with expected resolution of the magnetometer and tilt angle detector. Gravity measurements will be used to complement the magnetic data qualitatively.

Future works will report on real field measurements of the present instrument in comparison with a scalar magnetometer.

Acknowledgements. This work was supported in part by the Spanish National Space Program (DGI-MEC) project MEIGA-MET-NET under the Grant AYA2011-29967-C05-01. The authors wish to thank all the MetNet team for all the support.

References

Cai, J., Andersen, N. L., and Malureanu, C.: In-Field Practical Calibration of Three-Axis Magnetometers, Proceedings of the 2010 International Technical Meeting of the Institute of Navigation, San Diego, CA, 2010.

DTUsat: available at: http://www.dtusat.dtu.dk, last access: December 2010, 2014.

GID

4, 385–434, 2014

Fernández, A. B., Sanz, R., Covisa, P., Tordesillas, J. M., and Díaz-Michelena, M.: Testing the three axis magnetometer and gradiometer MOURA and data comparison on San Pablo de los Montes Observatory, vol. 15, EGU General Assembly 2013 Conference, Vienna, 2013.

Freitas, P. P., Ferreira, R., Cardoso, S., and Cardoso, F.: Magnetoresistive sensors, J. Phys.-Condens. Mat., 19, 165221, doi:10.1088/0953-8984/19/16/165221, 2007.

Geomagnetic observatories: available at: www.ign.es and www.intermagnet.org, last access: October 2013, 2014.

Honeywell Magnetic Sensors: Morristown, NJ, USA, available at: http://www.magneticsensors.com/magnetic-sensor-products.phpHoneywell, last access: October 2013, 2014.

Mars MetNet Mission: available at: http://metnet.fmi.fi, last access: October 2013, 2014.

Michelena, M. D.: Small Magnetic Sensors for Space Application, Sensors, 4, 2271–2288, 2009.

Michelena, M. D., Arruego, I., Oter, J. M., and Guerrero, H.: COTS-Based Wireless Magnetic Sensor for Small Satellites, IEEE T. Aerospace Elect. Syst., 46, 542–557, 2010.

Petrucha, V. and Kaspar, P.: 'Calibration of a Triaxial Fluxgate Magnetometer and Accelerometer with an Automated Non-magnetic Calibration System, 2009 IEEE Sensors Conference, Christchurch, New Zealand, 1510–1513, 2009.

Petrucha, V., Kaspar, P., Ripka, P., and Merayo, J.: Automated System for the Calibration of Magnetometers, J. Appl. Phys., 105, 07E704-1–07E704-3, 2009.

Renaudin, V., Afzal, M. H., and Lachapelle, G.: Complete Triaxis Magnetometer Calibration in the Magnetic Domain, J. Sensors, 2010, 967245, doi:10.1155/2010/967245, 2010.

Sanz, R., Cerdán, M. F., Wise, A., McHenry, M. E., and Díaz Michelena, M.: Temperature dependent Magnetization and Remanent Magnetization in Pseudo-binary $x(Fe_2TiO_4) - (1 - x)(Fe_3O_4)(0.30 < x < 1.00)$ Titanomagnetites, IEEE T. Magnet., 47, 4128–4131, 2011.

Sanz, R., Fernández, A. B., Dominguez, J. A., Martín, B., and Diaz-Michelena, M.: Gamma Irradiation of Magnetoresistive Sensors for Planetary Exploration, Sensors, 12, 4447–4465, 2012.

Sordo-Ibáñez, S., Piñero-García, B., Muñoz-Díaz, M., Ragel-Morales, A., Ceballos-Cáceres, J., Carranza-González, L., Espejo-Meana, S., Arias-Drake, A., Ramos-Martos, J., Mora-Gutiérrez, J. M., and Lagos-Florido, M. A.: A Front-End ASIC for a 16-Bit Three-Axis Magnetometer for Space Applications Based on Anisotropic Magnetoresistors, Design of Circuits and Integrated Systems (DCIS), accepted, 2013.

GID
4, 385–434, 2014

Table 1. MOURA characteristics summary.

Characteristics	Conditions	Min	Typical	Max	Unit
Sourcing voltage (V_{dd})		4.5	5	5.5	V
Set/reset voltage ($V_{s/r}$)		10	12	15	V
Sourcing current (I_{dd})	@ 5 V, RT, stand-by	81		86	mA
Set/reset current ($I_{s/r}$)	@ 12 V, RT		< 2		mA
Operating temperature		−100		70	°C
Storage temperature		−130		125	°C
Field range	Nominal		±65		µT
Extended range	Auto-offset compensation		±130		µT
Linearity error	Nominal range		< 0.5		% FS
Hysteresis error	Nominal range		< 0.1		% FS
Repeatability error	Nominal range		< 0.1		% FS
Sensitivity			0.45		Cts nT^{-1}
Resolution			2.2		nT
PSD	@ 0.5 Hz samples averaged: 1		0.85		nT $\sqrt{Hz}^{-1}$
	@ 0.5 Hz samples averaged: 10		0.42		nT $\sqrt{Hz}^{-1}$
	@ 0.5 Hz samples averaged: 100		0.28		nT $\sqrt{Hz}^{-1}$
Mass			72		g
Box dimensions			150 × 30 × 15		mm

GID
4, 385–434, 2014

Table 2. Channels involved in the study.

Sensor	Channel	Physical magnitude (units)
Sourcing voltage (V_{dd})	VREG	Voltage sourcing the magnetoresistive bridge (V)
Magnetic sensors axes	X1, X2, Y1, Y2, Z1, Z2	Magnetic field (nT)
Temperature sensors	TMP1, TMP2	Temperature (°C)

GID
4, 385–434, 2014

Table 3. Calibration of fluxgate megnetometers.

Parameter	Specified	FG-100			FG-500		
		X	*Y*	*Z*	*X*	*Y*	*Z*
Orthogonality error	(°) ± 0.1°	< 0.1′	< 0.1′	< 0.1′	< 0.1′	< 0.1′	< 0.1′
Offset error in zero field	(nT) F. S.	0	−1.5	1	1.5	−10	−0.5
Scaling error	(%) @ 35 Hz, ±0.5 %	0.08	0.03	−0.08	0.07	0.15	0.20
Frequency response	(%) ± 5 %	−0.06	0.06	0.08	1.00	1.17	1.05
Noise	($pT_{RMS}\sqrt{Hz^{-1}}$) @ 1 Hz	19.3	12.3	15.6	8.9	8.5	9.7

GID
4, 385–434, 2014

Table 4. Offset of magnetic sensors at room temperature.

Sensor 1	Offset (nT @ TMP1 = 18.13 ± 0.03 °C)
X1	764 ± 5
Y1	−1130 ± 6
Z1	1582 ± 8
Sensor 2	**Offset (nT @ TMP2 = 19.21 ± 0.03 °C)**
X2	1107 ± 3
Y2	−538 ± 5
Z2	1427 ± 7

GID
4, 385–434, 2014

Table 5.

Plane	Electrical current ($\omega = 1^{\circ}\,\mathrm{step}^{-1}$)	Sequence of steps
XY	$I_x(t) = 60\,\mathrm{mA} \cdot \cos(\omega \cdot \mathrm{step})$ $I_y(t) = 60\,\mathrm{mA} \cdot \sin(\omega \cdot \mathrm{step})$	From 1 to 360
ZX	$I_z(t) = 60\,\mathrm{mA} \cdot \cos(\omega \cdot \mathrm{step})$ $I_x(t) = 60\,\mathrm{mA} \cdot \sin(\omega \cdot \mathrm{step})$	From 361 to 721
YZ	$I_y(t) = 60\,\mathrm{mA} \cdot \cos(\omega \cdot \mathrm{step})$ $I_z(t) = 60\,\mathrm{mA} \cdot \sin(\omega \cdot \mathrm{step})$	From 722 to 1082

GID
4, 385–434, 2014

Table 6. Parameters δ and P of Eq. (4).

MOURA/ HC planes	δ (°)	P
X1Y1/XY	0.64 ± 0.05	−0.997 ± 0.001
X1Z1/XZ	7.3 ± 0.2	−0.986 ± 0.004
Y1Z1/YZ	−0.42 ± 0.2	1.005 ± 0.004
X2Y2/XY	1.76 ± 0.05	−0.997 ± 0.001
X2Z2/XZ	−5.3 ± 0.1	0.973 ± 0.002
Y2Z2/YZ	1.12 ± 0.1	−1.006 ± 0.003

GID
4, 385–434, 2014

Table 7. Gains at room temperature.

Sensor 1		Sensor 2	
$GAIN_{X1}$	0.910 ± 0.003	$GAIN_{X2}$	0.815 ± 0.003
$GAIN_{Y1}$	0.902 ± 0.002	$GAIN_{Y2}$	0.807 ± 0.001
$GAIN_{Z1}$	0.832 ± 0.003	$GAIN_{Z2}$	0.783 ± 0.002

GID
4, 385–434, 2014

Table 8. Tilt angles around $+X$ (α tilt angle) and experimental values (converted into g) for the first 5 steps.

α (°)	$\Delta\alpha$ (°)	ACC_X (g)	ACC_Y (g)	ACC_Z (g)	ACC (g)
4.9719	$< \pm 0.16$	0.2299	0.7839	−0.4297	0.92302
11.5369	$< \pm 0.16$	0.3043	0.7182	−0.4747	0.9131
19.4711	$< \pm 0.16$	0.3953	0.6261	−0.5170	0.9031
30.0000	$< \pm 0.16$	0.5080	0.4920	−0.5483	0.8948
41.8103	$< \pm 0.16$	0.6411	0.3583	−0.6114	0.9556

GID
4, 385–434, 2014

Table 9. Relative error between experimental and theoretical values of α for different α.

α (°)	ACC_X (g)	ACC_Y (g)	ACC_Z (g)	ACC (g)
5	2.7 %	−1.5 %	0.0 %	−0.9 %
12	3.5 %	−3.5 %	−0.5 %	−2.0 %
19	4.6 %	−6.8 %	−1.2 %	−3.1 %
30	4.8 %	−12.3 %	−2.8 %	−3.9 %
42	7.8 %	−15.0 %	5.4 %	2.6 %

GID
4, 385–434, 2014

Table 10. Temperature registers and their temporal variation.

Measurement	TT (°C)	TL (°C)	TMP1 (°C)	TMP2 (°C)
1	59.4 ± 0.1	58.9 ± 0.2	50.4 ± 0.1	50.04 ± 0.04
2	32.6 ± 0.2	32.2 ± 0.1	25.9 ± 0.1	25.6 ± 0.1
3	5.4 ± 0.2	4.1 ± 0.1	−0.3 ± 0.2	−0.6 ± 0.2
4	16.6 ± 0.1	17.3 ± 0.1	11.8 ± 0.2	11.55 ± 0.2
5	44.8 ± 0.1	45.4 ± 0.1	38.4 ± 0.1	38.2 ± 0.1
6	58.4 ± 0.2	58.8 ± 0.2	50.6 ± 0.1	50.51 ± 0.01

GID
4, 385–434, 2014

Table 11. Gain variations with temperature.

Axis ΔGAIN	Value ($^{\circ}C^{-1}$)
$\Delta GAIN_{X1}$	$-0.00370 \pm 5 \times 10^{-5}$
$\Delta GAIN_{Y1}$	$-0.00382 \pm 7 \times 10^{-5}$
$\Delta GAIN_{Z1}$	$-0.00384 \pm 4 \times 10^{-5}$
$\Delta GAIN_{X2}$	$-0.00591 \pm 5 \times 10^{-5}$
$\Delta GAIN_{Y2}$	$-0.00621 \pm 9 \times 10^{-5}$
$\Delta GAIN_{Z2}$	$-0.00616 \pm 6 \times 10^{-5}$

GID
4, 385–434, 2014

Table 12. Gains and thermal variations of gains, and offsets. Apart form the thermal variation of offset, equal to that of the gain, it has not been detected a drift within the time of test.

SENSOR 1 axis	GAIN @ T_G = TMP1 = 25.9 ± 0.2 °C	ΔGAIN (°C^{-1}) (referred to T_G)	OFFSET (nT) @ TMP1 = 18.13 ± 0.03 °C
X	0.910 ± 0.003	(−0.00370 ± 5 × 10^{-5})	764 ± 5
Y	0.902 ± 0.002	(−0.00382 ± 7 × 10^{-5})	−1130 ± 16
Z	0.832 ± 0.003	(−0.00384 ± 4 × 10^{-5})	1582 ± 8
SENSOR 2 axis	GAIN @ T_G = TMP2 = 25.6 ± 0.2 °C	ΔGAIN (°C^{-1}) (referred to TG)	OFFSET (nT) @ TMP2 = 19.21 ± 0.03 °C
X	0.815 ± 0.003	(−0.00591 ± 5 × 10^{-5})	1107 ± 3
Y	0.807 ± 0.001	(−0.00621 ± 9 × 10^{-5})	−538 ± 5
Z	0.783 ± 0.002	(−0.00616 ± 6 × 10^{-5})	1427 ± 17

GID
4, 385–434, 2014

Table 13. Inner coils constants at the different temperatures.

TMP1	Constant ($nT\,nT^{-1}$) ± 0.0003		
(°C ± 0.05)	X1	Y1	Z1
16.41	0.8879	0.9116	0.8617
49.55	0.7743	0.8022	0.7644
26.92	0.8518	0.8767	0.8293
0.69	0.9406	0.9656	0.9086
11.42	0.9045	0.9290	0.8760
37.53	0.8160	0.8414	0.7961
50.37	0.7722	0.7988	0.7564

GID
4, 385–434, 2014

Table 14. Sensor 1 inner coils characterization with temperature.

ΔConstant axis	Value $((\mathrm{nT\,nT^{-1}})/^{\circ}\mathrm{C}^{-1})$
$\Delta\mathrm{Constant}_{X1}$	$-0.088034 \pm 7 \times 10^{-6}$
$\Delta\mathrm{Constant}_{Y1}$	$-0.086506 \pm 1 \times 10^{-5}$
$\Delta\mathrm{Constant}_{Z1}$	$-0.078218 \pm 4 \times 10^{-5}$

GID
4, 385–434, 2014

Figure 1. MMPM mock up. The inset shows the position of MOURA sewed to the inflatable structure of the lander (red arrow).

GID
4, 385–434, 2014

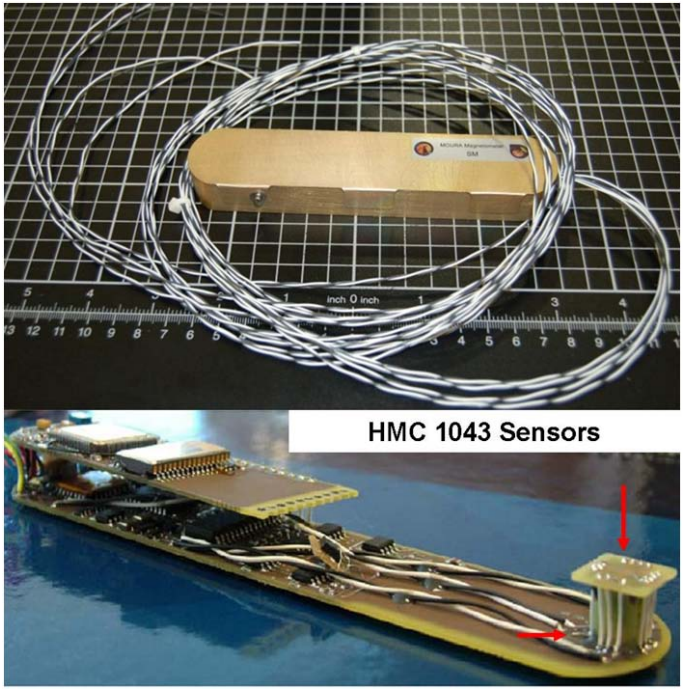

Figure 2. QM-MOURA box and detailed view of position of both HMC1043 sensors (red arrows).

GID
4, 385–434, 2014

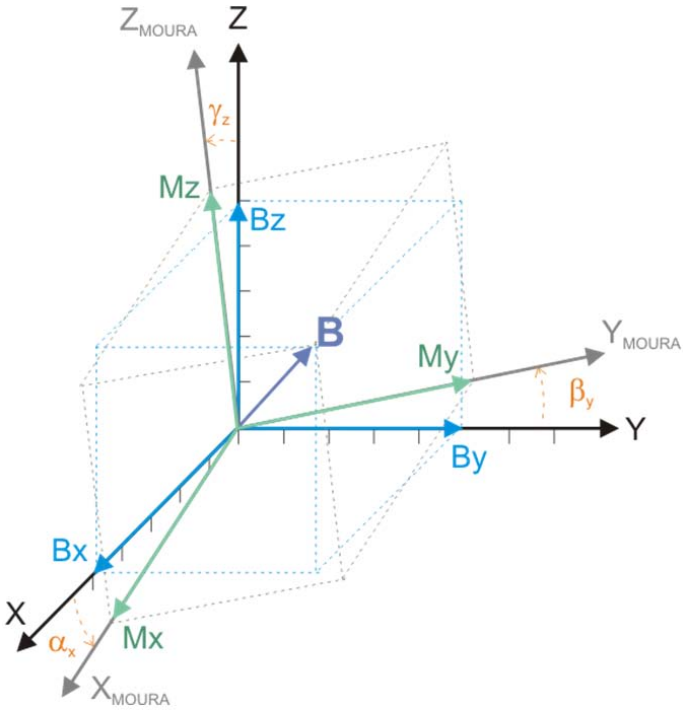

Figure 3. Approximation of system of reference of MOURA vs. external system of reference with approximation taken into account.

GID
4, 385–434, 2014

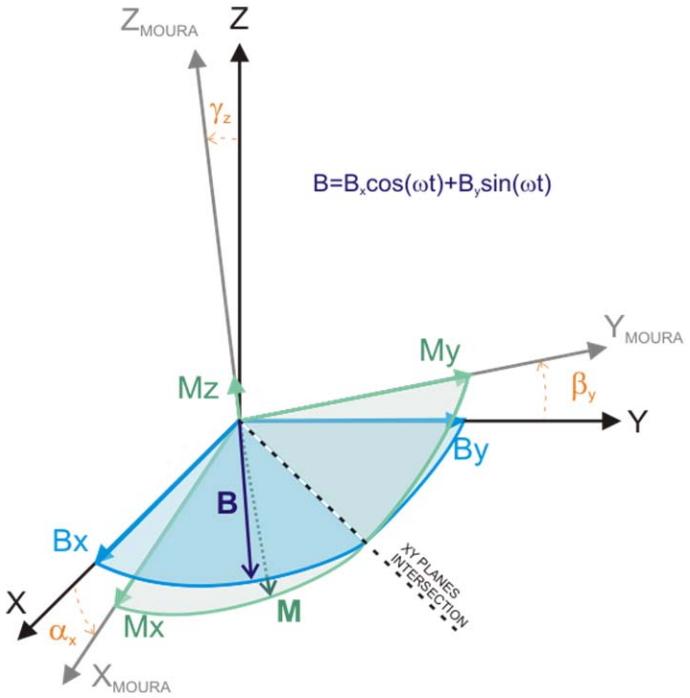

Figure 4. Sketch of the different shapes of magnetic field measured in external and MOURA reference system.

GID
4, 385–434, 2014

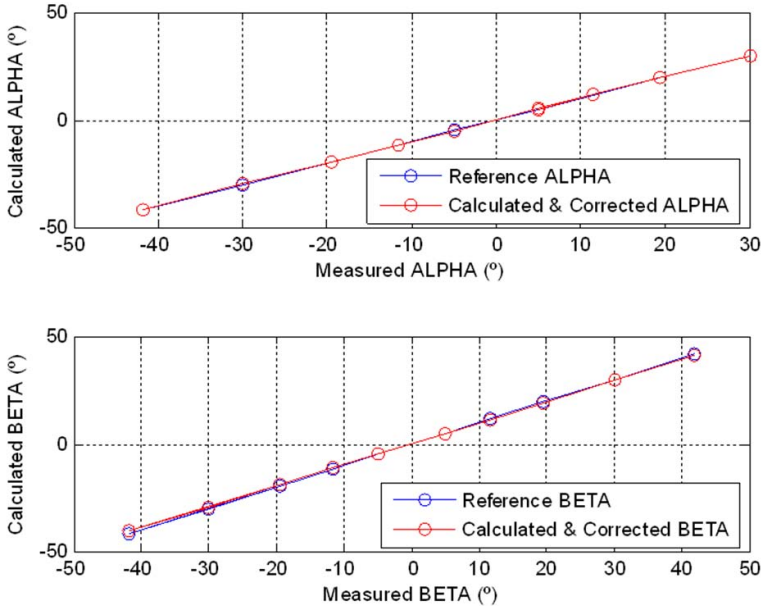

Figure 5. Corrected values of the tilt angles.

GID
4, 385–434, 2014

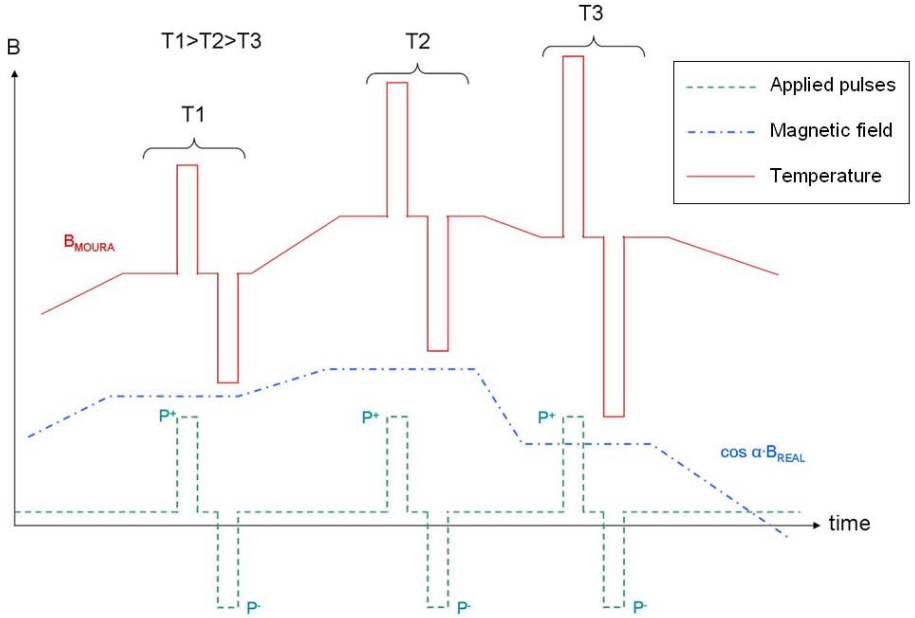

Figure 6. Sketch of applied pulses, real external magnetic field, registred signal by MOURA for different temperatures (T1, T2 and T3) as a function of time.

GID
4, 385–434, 2014

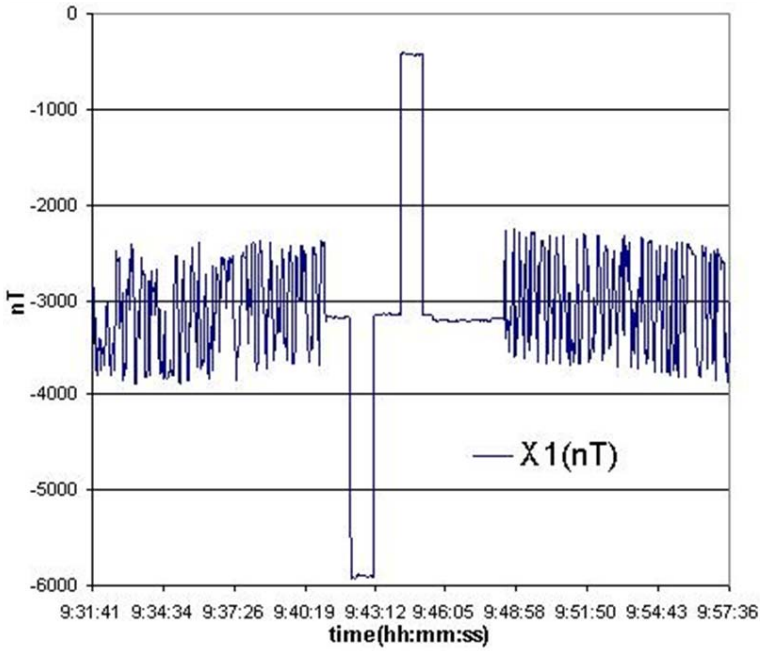

Figure 7. Detailed view of the register data by Sensor 1 *x* axis, minutes before and after the application of magnetic pulses (thermal chamber ON-OFF).

GID
4, 385–434, 2014

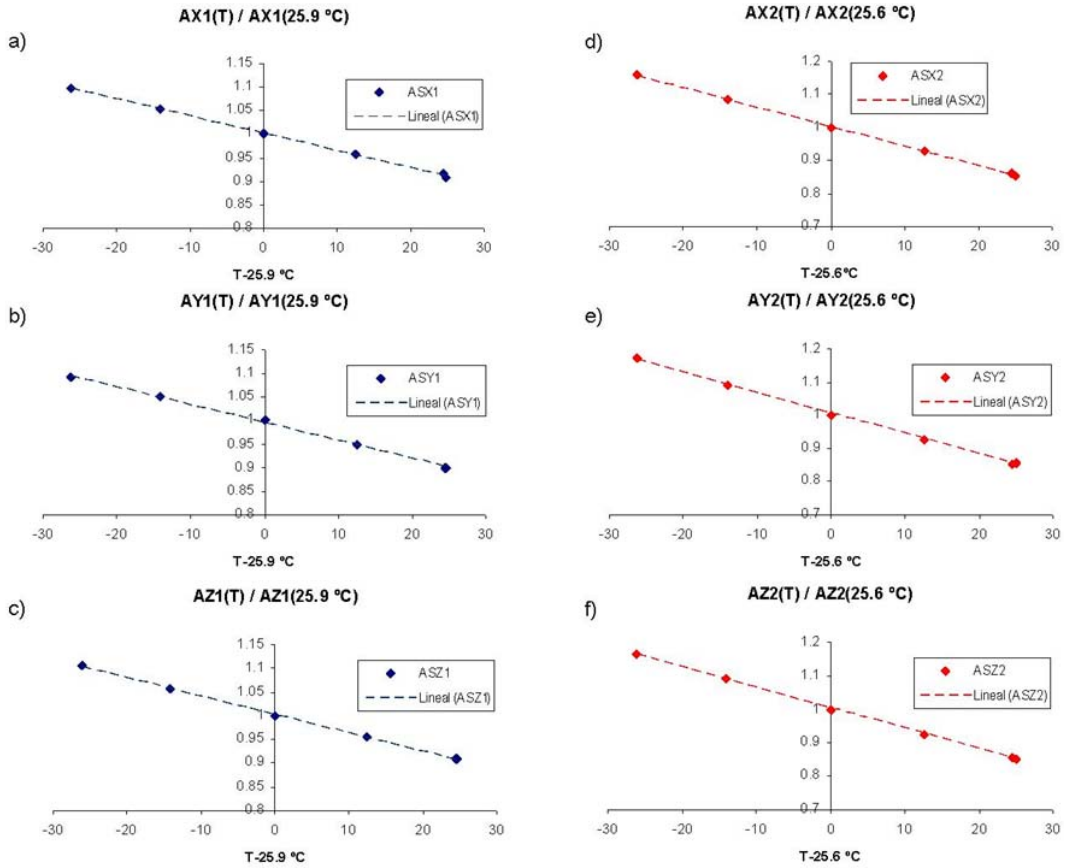

Figure 8. Normalized amplitude as a function of modified temperature for axis sensor **(a)** X1, **(b)** Y1, **(c)** Z1, **(d)** X2, **(e)** Y2, **(f)** Z2.

GID
4, 385–434, 2014

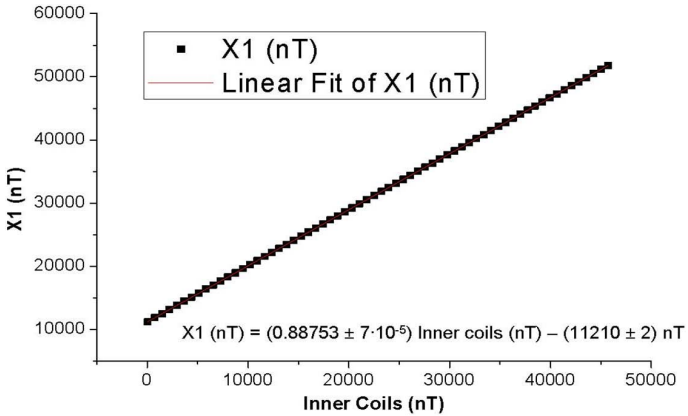

Figure 9. Data of Sensor 1 *x* axis "Ramp I" at 16.41 °C (TMP1).

GID
4, 385–434, 2014

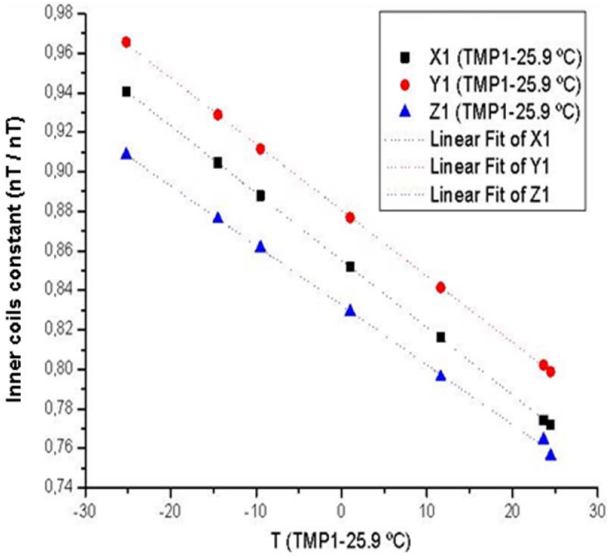

Figure 10. Linear fits of gain as a function of corrected temperature (TMP1-Tref).

GID
4, 385–434, 2014

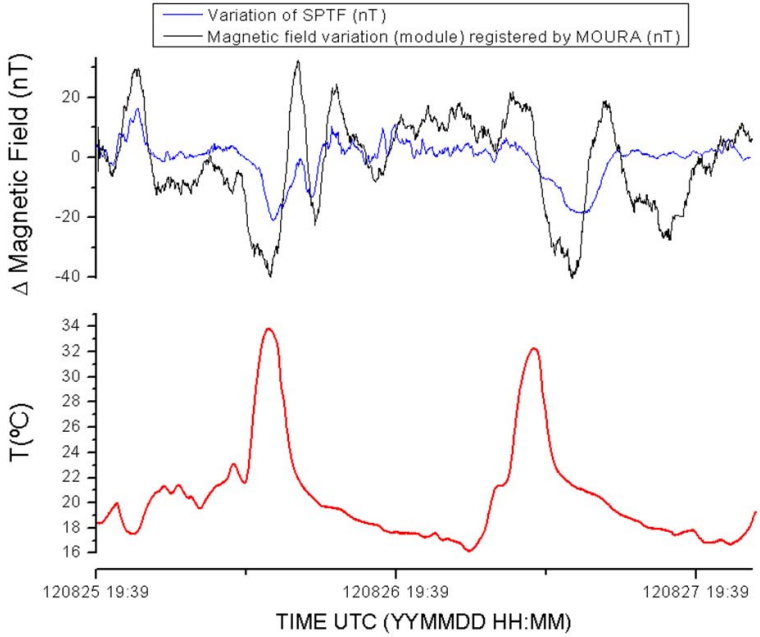

Figure 11. Registered variation of modulus of magnetic field by sensor 2 of MOURA vs. magnetic field registered by San Pablo de los Montes Geomagnetic Observatory. Black line is an 11 point averaging of MOURA signal.

GID
4, 385–434, 2014